

Liquid Crystal Order in Colloidal Suspensions of Spheroidal Particles by Direct Current Electric Field Assembly

Aayush A. Shah, Heekyoung Kang, Kevin L. Kohlstedt, Kyung Hyun Ahn, Sharon C. Glotzer, Charles W. Monroe, and Michael J. Solomon*

DC electric fields are used to produce colloidal assemblies with orientational and layered positional order from a dilute suspension of spheroidal particles. These 3D assemblies, which can be visualized in situ by confocal microscopy, are achieved in short time spans ($t < 1$ h) by the application of a constant voltage across the capacitor-like device. This method yields denser and more ordered assemblies than had been previously reported with other assembly methods. Structures with a high degree of orientational order as well as layered positional order normal to the electrode surface are observed. These colloidal structures are explained as a consequence of electrophoretic deposition and field-assisted assembly. The interplay between the deposition rate and the rotational Brownian motion is found to be critical for the optimal ordering, which occurs when these rates, as quantified by the Peclet number, are of order one. The results suggest that the mechanism leading to ordering is equilibrium self-assembly but with kinetics dramatically accelerated by the application of the DC electric field. Finally, the crystalline symmetry of the densest structure formed is determined and compared with previously studied spheroidal assemblies.

A. A. Shah, S. C. Glotzer, Prof. M. J. Solomon
Program of Macromolecular Science and Engineering
University of Michigan
Ann Arbor, MI, USA
E-mail: mjsolo@umich.edu

A. A. Shah, S. C. Glotzer
Department of Materials Science and Engineering
University of Michigan
Ann Arbor, MI, USA

H. Kang, K. H. Ahn
School of Chemical and Biological Engineering
Seoul National University
Seoul, Korea

K. L. Kohlstedt, S. C. Glotzer, C. W. Monroe, Prof. M. J. Solomon
Department of Chemical Engineering
University of Michigan
3410 G.G. Brown, 2300 Hayward Street
Ann Arbor, MI 48109-2136

DOI: 10.1002/sml.201102265



1. Introduction

Anisotropic colloidal particles^[1] have the potential to assemble into structures with complex symmetries, such as the body-centered cubic (bcc) rotator phase,^[2] diamond,^[3,4] and other non-orthorhombic symmetries.^[5] In addition, anisotropic particles can adopt preferential orientations on the lattice positions of these self-assembled crystals.^[6] Such complex unit cells have applications in advanced optical materials.^[7] Further, the orientational alignment of the anisotropic building blocks is also important for new forms of matter, such as metamaterials^[1,8] and reconfigurable colloids.^[9] Spheroids are simple anisotropic building blocks that may adopt both positional and orientational order in crystal structures. A practical advantage of using spheroids for experimental studies is their convenient production via syntheses based on the solidification of liquid droplets.^[10–13]

For hard prolate spheroids, the classic simulations of Frenkel and Mulder found a progression of stability

with increasing volume fraction from the isotropic phase, to the nematic phase, to an oriented crystal, with a unit cell having face-centered orthorhombic (fco, uniaxially stretched face-centered cubic (fcc)) symmetry.^[6] The recent results of Pfleiderer and Schilling,^[14] building on the packing simulations of Donev et al.,^[15,16] have found a higher-density, entropically stabilized monoclinic phase. This phase breaks cubic symmetry and has a two spheroid centered monoclinic unit cell (*mC2*) mutually aligned at an angle that depends on the packing fraction of the suspension.^[15] While further free-energy studies were done to quantify the self-assembly propensity of hard spheroids to the *mC2* phase,^[17] such systems have proved difficult to assemble rapidly.^[18]

Although these structures are important targets for self-assembly and a number of them have been observed experimentally,^[19] micrometer-scale rods with prolate spheroidal or cylindrical shape are difficult to self-assemble because of their slow translational and rotational Brownian motion. For example, the isotropic–nematic transition can require more than 24 h for cylindrical rods of length 180 nm^[20] and simulations predict significant barriers to the nucleation of multilayer structures.^[21] Thus, methods to accelerate the self-assembly of anisotropic colloids are required.

Analogous to methods to accelerate crystallization of spheres,^[22–24] gravitational, electric, convective flow, or shear fields may be applied to accelerate ordering in suspensions of anisotropic particles.^[25] By varying the strength of the applied field, orientational order of colloidal rods was previously generated with an effective gravitational force generated by centrifugation.^[18] However, in that study the field-strength was too large (Peclet number, $Pe \gg 1$) to give high-quality ordering or allow a direct connection to self-assembly. Electric fields are a promising alternative compared to centrifugation for field-assisted assembly because they can be applied across a variety of geometries, including those compatible with in situ visualization of the assembly process.

To date, AC electric fields have been the predominant means to generate chains and 2D crystals from rods and spheres.^[26–32] Such dielectrophoretic methods can be extended to yield 3D assemblies when the gap between the electrodes is thin.^[30,31] AC electric fields require relatively high electric fields. In this paper we address the rapid assembly of prolate spheroidal colloids through the novel use of a DC electric field-assisted assembly device. We characterize the assembled phases using confocal microscopy.

This method is based on the application of small electric fields generated by relatively low applied voltages (~1–3 V). The DC electric field couples to the charge monopole of the rods, generating electrophoretic motion of the particle.^[24,33,34] This electrophoretic motion densifies the colloidal suspension at the electrode whose polarity is opposite to that of the spheroidal particles. It is important to emphasize that the low voltage electric field does not align the spheroids, but rather provides a driving force towards denser configurations. The densification is sufficient to induce a phase transition that persists many (>15) colloidal layers away from the electrode surface. We observe highly aligned nematic structures, as well as layered positional ordering of the prolate spheroids along

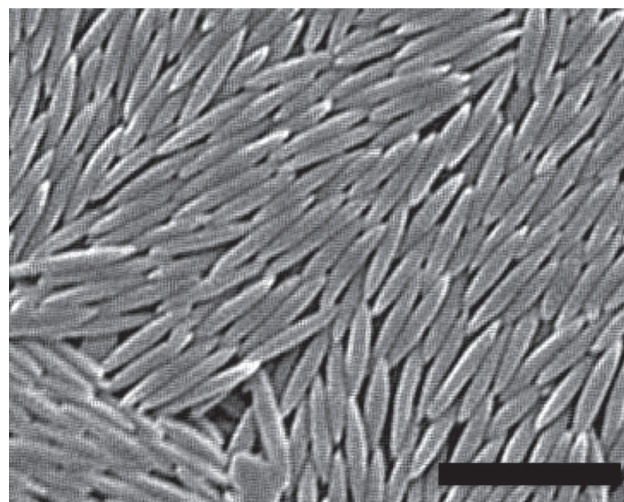


Figure 1. SEM image of polystyrene ellipsoids. Their aspect ratio is 4.3 ± 0.6 . Major axis $L = 3.35 \pm 0.41 \mu\text{m}$ and minor axis $D = 0.79 \pm 0.07 \mu\text{m}$. Scale bar is $5.0 \mu\text{m}$.

an axis parallel to the electrode surface at the highest packing fraction.

2. Results

We directly visualize the assembly of polystyrene (PS) spheroidal particles of aspect ratio 4.3 ± 0.6 (major axis $L = 3.35 \pm 0.41 \mu\text{m}$ and a minor axis $D = 0.79 \pm 0.07 \mu\text{m}$). The particles are relatively uniform in size and shape, as shown in the scanning electron microscopy (SEM) image of **Figure 1**. They were produced by uniaxial deformation of PS spheres embedded in an elastomeric film (see Methods Section). We use the electrolyte tetrabutylammonium chloride (TBAC, 0.1 mM) to screen the electrostatic interactions between the particles. The Debye length (κ^{-1}) was found to be 23.9 nm from a conductivity measurement of the system ($3.45 \mu\text{S/cm}$). For some measurements, a small amount of photopolymer and initiator was added to the solvent to allow the assembled structure to be immobilized by UV-induced photopolymerization for further direct visualization studies (see the Methods Section). The ζ -potential of the colloids at the conditions of the experiments was measured to be $-38 \pm 12 \text{ mV}$.

A small volume ($\sim 35 \mu\text{L}$) of the colloidal rod suspension at an initial volume fraction $\phi_1 = 2.0\%$ was placed between parallel planar electrodes (indium tin oxide (ITO) coated on glass coverslips) held at a separation of 1.15 mm with a glass spacer. The cross-sectional area available for assembly was 19.6 mm^2 . The device, which resembles a parallel-plate capacitor, was mounted on the stage of a confocal laser scanning microscope (CLSM, Leica TCS-SP2) for in situ visualization with a numerical aperture, $NA = 1.4$ oil immersion objective. The two electrodes were connected to a potentiostat (Autolab PGSTAT 128N), which applied a constant voltage and measured the resultant current density. A schematic of the device is shown in **Figure 2a**. Images of the assembled cell and the area available for self-assembly are shown in

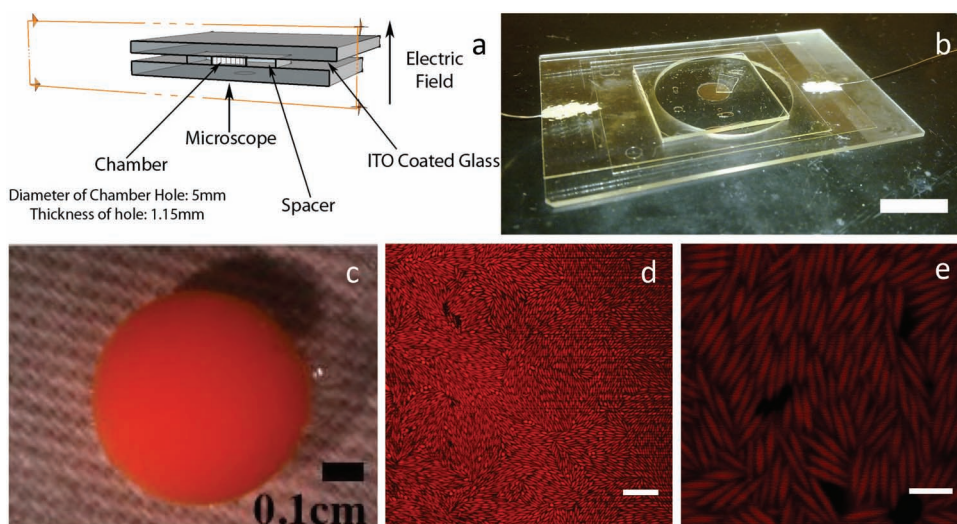


Figure 2. a) Schematic of the DC electric field device used to assemble colloidal rods. The electrode gap is 1.15 mm. b) Image of device. Scale bar is 1.0 cm. c) Image of the chamber containing the colloidal suspension. The central region is orange due to fluorescence on the suspended rods. Scale bar is 0.1 cm. d) Zoomed-out CLSM image of an assembly generated by the electrical field device. The assembly is obtained on application of a constant 2.0 V and the image is at the electrode surface. Orientational ordering on large scales is apparent. Scale bar is 20.0 μm . e) A zoomed-in CLSM image of the same experiment. It shows the orientational alignment of individual rods. Scale bar is 3.0 μm .

Figure 2b,c. Representative confocal microscopy images of self-assembled structures obtained *in situ* are shown for field of views of 161 $\mu\text{m} \times 161 \mu\text{m}$ (Figure 2d) and 19 $\mu\text{m} \times 19 \mu\text{m}$ (Figure 2e).

We tested the device using spherical particles to create a 3D close-packed crystal (see Supporting Information, SI) consistent with earlier reports that used similar methods.^[24,34] We then introduced spheroidal particles at an initial volume fraction of 2.0%. On application of a constant DC voltage, the negatively charged spheroids migrated towards the positively charged electrode. The transient densification of the PS rods in dimethyl sulfoxide (DMSO) was observed at the coverslip by imaging at 1.4 fps using the CLSM. Images that characterize the kinetics of rod assembly are shown in **Figure 3** and in Movie 1 (SM1 in the SI). Figure 3a shows that the sample was initially unaligned and at a low volume fraction. The densification process began upon application of the constant voltage. After about 3 min (Figure 3b), the first regions of enhanced rod concentration were observed, although these regions are still largely disordered both in position and orientation. SM1 shows that the enhancement of colloidal density was due to particles moving into the image focal plane (from above). Movie 2 (SM2 in the SI) shows the rod assembly under the same conditions as Figure 3 and SM1, but visualized in a plane perpendicular to the electrode surface. SM2 also shows that the increase in colloidal density at the electrode surface is due to the migration of rods toward the electrode surface from the bulk of the sample.

For 1.5 min $< t < 7$ min, the sample continued to densify over time as the regions of concentrated disorder grew (Figure 3c). Even though densification of the rods due to deposition occurred in this period, the rods remained highly mobile due to Brownian translations and rotations at this voltage and volume fraction (see SM1 in the SI).

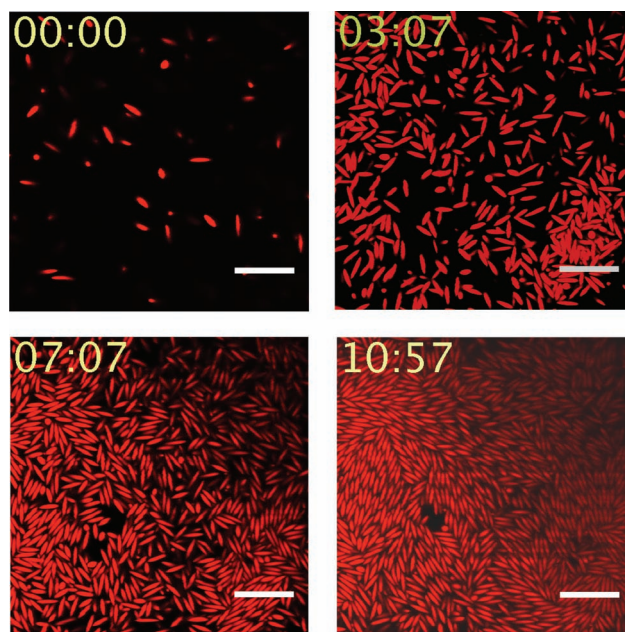


Figure 3. Images show the kinetics of the self-assembly of colloidal rods as observed by confocal microscopy at 1.85 V. Time values, t , in minutes and seconds are indicated in the upper left corners. The initial volume fraction is 2%. The images, acquired in a plane parallel to the electrode surface, show that the volume fraction and orientational order increase over time, until a nematic phase is apparent after the electric field has been applied for about 11 min. The scale bars are 10.0 μm .

The rod suspension showed significant alignment (Figure 3d) at $t \sim 11$ min which persisted until the conclusion of the experiment ($t = 1.5$ h). The structure of the suspension appeared visually to be nematic, with a domain texture visible on scales of 5 μm . SM2 indicates that the orientational

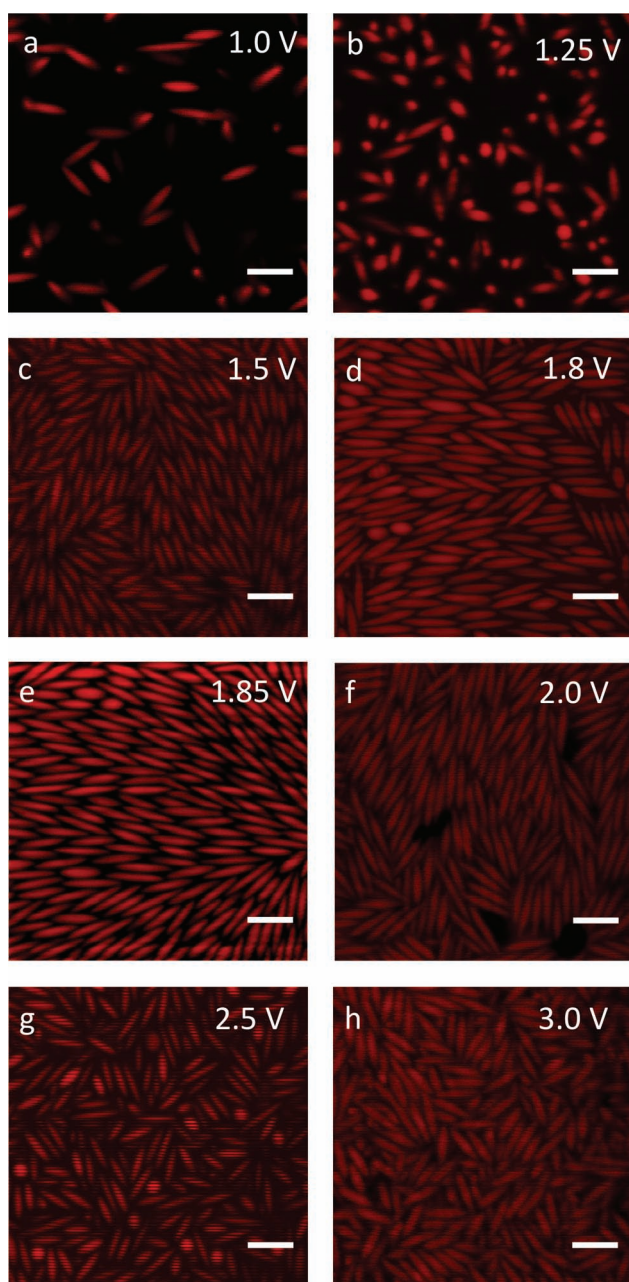


Figure 4. CLSM images of the self-assemblies acquired at the electrode surface after the structures have achieved steady state. Assemblies are obtained on application of different constant voltages (a–h). Scale bars are 3 μm .

order extends at least 8 μm into the specimen. We further observed ordering up to at least 15 μm into the sample by imaging the suspension at the highest excitation power of the CLSM. This distance is at the limit for imaging in this system, given the refractive-index contrast between the PS particles and the DMSO solvent. Ordering may have continued above this distance; however, it could no longer be observed in this particular colloid/solvent system.

Figure 4 shows the effect of different applied voltages on the rod assemblies. The samples were imaged at the surface of the positive electrode after at least 1 h. This time was

sufficient for the system to reach a steady-state structure, as per the kinetics reported previously in Figure 3.

Figure 4a and b show that this structure is orientationally and positionally disordered at applied voltages of 1.0 and 1.25 V. (Regions of the images with radially symmetric intensity resembling that of a sphere are actually rods oriented perpendicular to the image plane and electrode surface.) Moreover, at these applied voltages, the rod assemblies were highly mobile due to Brownian motion. The solvent of these specimens was photopolymerized during assembly to lock in the structure prior to 3D CLSM imaging. This procedure made quantification of order possible in these highly mobile assemblies (see Methods Section). Figure 4c shows that an applied voltage of 1.5 V results in a much denser colloidal phase at the electrode surface than that observed for the lower applied voltages, with some aligned domains. However, the layers further above the electrode (not apparent in Figure 4c) are more disordered and diffuse.

In Figure 4d and e, we show assemblies with a high degree of alignment for applied voltages of 1.80 and 1.85 V, respectively. Here, the effect of the applied voltage was sufficient to support significant densification of the colloidal particles at the electrode surface.

As the applied voltage was increased to 2 V, small domains of order were evident (Figure 4f), but there was no large-scale order. At 2.5 and 3.0 V, the rods appeared jammed, with limited mobility due to the rapid densification caused by the high initial voltage. Moreover, the assemblies in Figure 4g and h do not show significant orientational or positional order.

Thus, variation of the applied voltage results in a series of reversible transitions among assemblies of colloidal spheroids. Lower applied voltages (<1.75 V) lead to fluids with orientational disorder. At intermediate applied voltages, nematic order as well as positional order is observed along an axis perpendicular to the electrode surface. Lastly, at large voltages (>2.5 V), a jammed, disordered packing of rods is formed.

We explain the rich assembly behavior in Figure 4 by investigating the effects of the electric field on the colloidal suspension. A spatially varying external field leads to a gradient in the osmotic pressure of the solution.^[35,36] Thus, the force due to the DC electric field is balanced by the gradient in osmotic pressure according to

$$\frac{d\Pi(z)}{dz} = -\frac{F_e}{V_p}\Phi(z) \quad (1)$$

Here, $\Pi(z)$ is the osmotic pressure as a function of the distance z from the electrode surface, F_e is the external force on the spheroid due to the DC electric field, V_p is the volume of the prolate spheroid, and $\Phi(z)$ is the volume fraction of rods at that height. In a semi-infinite medium, integration of Equation 1 and application of the boundary condition $\Pi(z \rightarrow \infty) = 0$ yields the osmotic pressure at the base of the sample^[35]

$$\Pi(z=0) = -\frac{F_e H}{V_p}\phi_i \quad (2)$$

We take the force on the particle to depend on the effective electric field E in the device (see SI). In the Smoluchowski

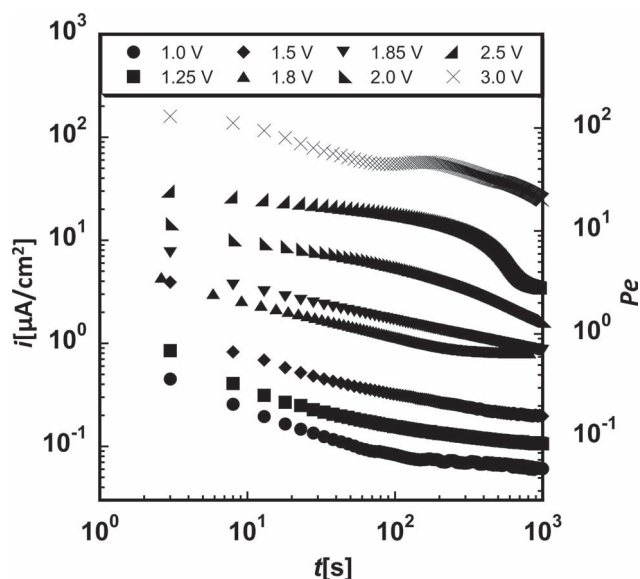


Figure 5. Time-dependent current density as measured upon application of different constant voltages across DMSO containing 0.1 mM tetrabutylammonium chloride salt. The measured current density is proportional to Pe (see text for definition), which is plotted on the right axis.

limit we can directly write $F_e = \epsilon \epsilon_0 \zeta A_r E$, where ϵ is the dielectric constant of the solvent, ϵ_0 is the permittivity of free space, ζ is the zeta potential, and $\langle A_r \rangle$ is the shape factor given in the SI.^[37] The effective electric field in the solution between the electrodes can be calculated through direct measurement of the current density for all the conditions reported in Figure 4. We neglected concentration polarization in calculating the effective electric field because we estimate that it is small relative to the voltages applied. For all electrode geometries, measured current density relates to the bulk electric field through:^[38]

$$\mathbf{E} = \frac{\mathbf{i}}{\lambda_0} \quad (3)$$

where \mathbf{i} is the current density (per area of electrode) generated in the device and λ_0 is the ionic conductivity of the solution

Results of the potentiostat measurements are reported in **Figure 5**. The measurements reported are for particle-free experiments, where i is measured in a test cell containing DMSO solvent and salt (TBAC). No significant differences in i were found using a 0.5 vol% solution of colloidal spheres or a 2.0 vol% solution of colloidal rods (data not shown). Measurements were conducted for 1000 s, the period required to generate steady-state assemblies in the device, as reported in Figure 3.

In Figure 5, for low applied voltages (1.0, 1.25 V), the current density generated was small ($<0.5 \mu\text{A}/\text{cm}^2$). The current density at 5 s corresponds to an effective field of 0.15 V/cm. For intermediate field strengths (1.5, 1.8, 1.85, 2.0 V), the current generated increased with voltage and was at least 10 times higher than measured for small field strengths ($i = 5 \mu\text{A}/\text{cm}^2$). The effective field for this range of applied

voltages was $\sim 1.5 \text{ V}/\text{cm}$. At the highest field strengths of 2.5 and 3.0 V, large initial current densities were observed ($>10 \mu\text{A}/\text{cm}^2$) and the effective field for these experiments was 7.5 V/cm for the initial currents.

The trends in Figure 5 are crucial to the understanding of the rod assembly experiments shown in Figure 4. First, the current is a monotonically increasing function of the applied voltage. This increase is expected from electrochemical kinetics, where current increases exponentially with voltage for the case of an electrode surface reaction.^[38] Further, at each applied voltage, the current progressively decreases over the duration of the experiment. This is consistent with electrochemical transport theories, in which i decreases with time for a fixed voltage due to mass transfer transients in the diffusion layer near the electrodes and depletion of the reactant in the bulk solution.^[38] Although a steady-state current density is not achieved, i stabilizes into a slow decay by $t = 100 \text{ s}$. This stabilization is faster than the kinetics of the assembly experiments that led to the results in Figure 3 and 4. At high voltages (2.5, 3.0 V), the steady state is achieved at later times ($t > 800 \text{ s}$) and most of the deposition and assembly has already occurred by this time. Although the range of voltages used varied only between 1.0–3.0 V, the difference in i (and thus effective fields) generated under these conditions varied by more than three orders of magnitude. The driving force due to the electric field experienced by the rod colloids is thus an extremely sensitive function of the applied voltage.

We find that the primary mechanism for the enhanced number density of colloids at the electrode surface is electrophoresis. DC electric fields are known to cause bulk fluid flows, which have an effect on particle mobility.^[33,39] To evaluate the possible significance of these previously reported fluid flows for our experiments, we applied a constant voltage across a test suspension of dilute spherical PS particles. The time-dependent displacement of the spheres ($\sigma = 1.1 \mu\text{m}$) was quantified by means of image processing and trajectory linking algorithms (see Methods Section). In the Smoluchowski limit, the electrophoretic mobility U is proportional the magnitude of the electric field $E = |\mathbf{E}|$

$$U = \frac{\epsilon \epsilon_0 \zeta E}{\eta} \quad (4)$$

where ϵ is the dielectric constant of the solvent, ϵ_0 is the permittivity of free space, ζ is the zeta potential, and η is the viscosity of the solution.

Equation 3 and 4 can be used to calculate the expected electrophoretic mobility from the measured current density and standard electrokinetic theory appropriate to the screening length of our system in the Smoluchowski limit. We find good agreement between the theoretical and experimental values of the electrophoretic velocity (the average relative error is 11%, see SI).

Thus, in our hypothesis, the electric field has an effect on the colloidal rod trajectories only to the extent that the electrophoretic displacement is dominant relative to the random motion of the rods due to rotational and translational Brownian motion. This physical idea allows us to parameterize the strength of the electric field by means of the

Peclet number (Pe), which can be interpreted as a ratio of the spheroid's characteristic rates of motion. In this work, Pe is the ratio of the rate of displacement of the colloid in the applied field to the rate of Brownian motion, evaluated at the scale of the longest dimension of the particle. Thus,

$$Pe = \frac{U/L}{D_r} = \frac{\varepsilon \varepsilon_0 \zeta E}{\eta L D_r} \quad (5)$$

where D_r is the rotational diffusivity, and again L is the length of the spheroid's major axis. The Pe is independent of viscosity because both the electrophoretic velocity and rotational diffusivity are inversely proportional to the viscosity.

From the theory of Brenner,^[40] we compute the rotational diffusivity of the prolate spheroids to be $D_r = 0.08 \pm 0.02 \text{ s}^{-1}$. The (time-dependent) Pe computed from the measured i for each of the constant-voltage experiments is reported in Figure 5.

In order to investigate trends in self-assembly with Pe , we take its value at a time of 100 s as characteristic of that applied voltage. Although a full analysis would account for the temporal evolution of Pe , the selection of Pe ($t = 100 \text{ s}$) as a characteristic value is supported in two ways. First, the time-dependent $i(t)$ (and thus Pe) had typically stabilized at nearly its steady-state value by $t = 100 \text{ s}$ for all voltages other than 2.5 and 3 V. Excluding these voltages, the measured i (and Pe) decreased on average by a factor of about 2.5 between $t = 100 \text{ s}$ and $t = 1000 \text{ s}$. This change is much smaller than the initial change of greater than a factor of 10 between $t = 0 \text{ s}$ and $t = 100 \text{ s}$. Second, the steady-state structures observed in Figure 4 were all achieved within the window of $100 \text{ s} < t < 1000 \text{ s}$. Even though a steady state is not reached in this time range for high voltages (2.5, 3.0 V), most of the assembly is complete due to the enhanced deposition rate. Thus, in subsequent figures we report Pe at $t = 100 \text{ s}$ as characteristic of the conditions for self-assembly. Understanding the specific effect of the time-dependence of the Pe would be of interest, but is beyond the scope of the current study.

By comparing the results of Figures 4 and 5, it is clear that the electric field was not sufficiently strong to densify the suspensions to the order–disorder transition for $Pe < 0.1$. Conversely, for $Pe > 1$, the motion due to the applied field dominated over the randomizing effects of Brownian motion and as a result, the particles had insufficient mobility to organize into orientationally ordered structures. Instead, orientationally and positionally ordered structures are only observed for $Pe \sim 1$, when rapid densification is still observed at the coverslip, but rotational and translational Brownian motions are still possible, thus permitting equilibration into ordered phases.

We used image-processing (IP) algorithms to quantify the observed ordering by identifying the centroids and orientation angles of all the rods in image volumes as acquired by confocal microscopy (see Methods Section).^[13] The volume imaged was $19.7 \mu\text{m} \times 19.7 \mu\text{m} \times 2.5 \mu\text{m}$. It extended out into the specimen from the positive electrode surface. We quantified the volume fraction for our assembly structures in the near-wall region ($z < 2.5 \mu\text{m}$) from the rods identified by image processing. From Figure 6a, the volume fraction is

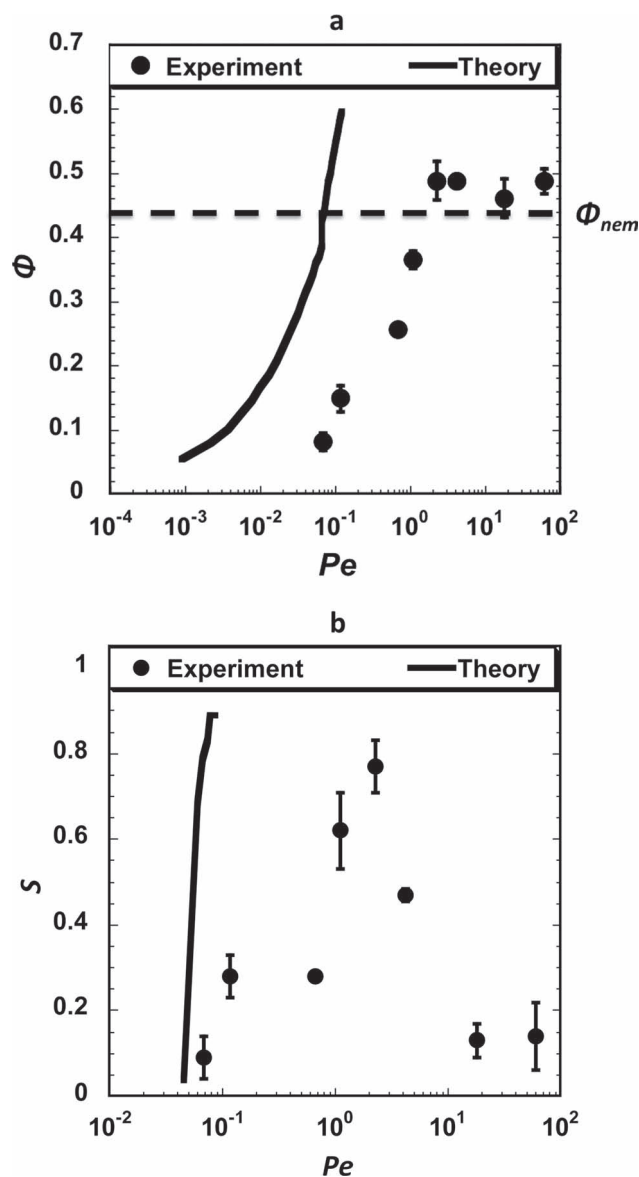


Figure 6. a) Volume fraction of the assembly structure of a $19.7 \mu\text{m} \times 19.7 \mu\text{m} \times 2.5 \mu\text{m}$ stack is plotted for Pe ($t = 100 \text{ s}$). The measured volume fractions are also compared to expected isotrope–nematic transition volume fractions from theory (dashed line).^[41] b) The nematic order parameter, S , is plotted for a $19.7 \mu\text{m} \times 19.7 \mu\text{m} \times 2.5 \mu\text{m}$ stack for different Pe ($t = 100 \text{ s}$) obtained on application of different initial voltages. Nematic ordering is observed when the Pe is ~ 1 . These results are compared to the order parameter predicted from application of Equation 7 and the results of equilibrium self-assembly simulations (solid lines).^[41]

initially an increasing function of Pe . For $Pe < 0.1$, the colloidal volume fraction is well below the phase transition. The volume fraction exceeds the phase transition coexistence region at $Pe \sim 1$ and stays nearly constant for the jammed structures obtained for $Pe > 1$.

We compare our assembly to that predicted by the theory of simple field-assisted assembly of Equation 1 and 2. The theory predicts the sediment volume fraction and order parameter to be a consequence of the osmotic pressure built

up in the sample so as to balance the force applied to the colloids by the electric field. In this case, we can write an implicit equation connecting the spheroid volume fraction to the Pe , through calculation of the osmotic pressure:

$$Pe = \frac{\Pi(z) V_p}{(A_r) \varphi_i H \eta L D_r} \quad (6)$$

The simulations of Tjijto–Margo and Evans^[41] report the osmotic pressure as a function of the volume fraction for a system of hard spheroids. With these results and Equation 6, we compute and plot the predicted dependence of the assembly volume fraction on the applied Pe . When compared to this field assisted self-assembly theory, we find that the experiments require an order of magnitude greater Pe than theoretically predicted to attain the volume fraction required for nematic order, as shown in Figure 6a.

We also computed the nematic order parameter S to quantify the quality of the orientational ordering. S is the largest eigenvalue of the orientation angle tensor, \mathbf{Q} , of all the rods in the image volume.

$$\mathbf{Q} = \frac{1}{2n_r} \sum_{i=1}^{n_r} 3\mathbf{d}_i \mathbf{d}_i - \mathbf{I} \quad (7)$$

where n_r is the number of rods in the image volume, \mathbf{d}_i is the director specifying the orientation angle of the i^{th} rod and \mathbf{I} is the identity tensor. S varies from 0 (complete orientational disorder) to 1 (full orientational order).

As is evident from Figure 6b, $S < 0.4$ for low dimensionless applied fields ($Pe < 0.1$). This quantification agrees well with the images reported in Figure 4a–c (Figure 4c shows small nematic domains in the colloidal layer immediately above the coverslip. However, the order parameter in these volumes is low because there is no overall 3D orientational order). Significant rod alignment ($S > 0.6$) was found for the intermediate Pe , again in good agreement with the images of Figure 4d and e. Structures with partial alignment ($S = 0.42$) were observed at the still higher applied voltage corresponding to $Pe = 2.5$ (see Figure 4f). Finally, we observe structures with small orientational order and glassy dynamics for $Pe > 10$. These conditions lead to low order parameter measurements ($S < 0.4$). In summary, through the calculation of S , the best rod orientational ordering was observed for $Pe \approx 1$ where the electrophoresis driving force is comparable to that of Brownian motion.

The order parameter for a given volume fraction of a self-assembling system of hard rods is also available from Tjijto–Margo and Evans.^[41] We use their data together with Equation 6 to predict the expected field-assisted assembly order parameters as a function of Pe . We find that the experimental order parameters are nearly as large as the theory predicts, but the Pe required to attain nematic ordering is ~ 10 times greater for the experiments than for the theory.

Thus, volume fraction and order parameter are highly correlated and consistent with equilibrium thermodynamics. However, the field strengths necessary to densify and align colloidal suspensions are about an order of magnitude greater than predicted by the simple theory of Equation 1 and 2

predicts. A similar discrepancy was reported by Mukhija and Solomon^[18] for the case of an effective gravitational field generated due to centrifugation.

The experiments and image processing also yield the centroid locations of all the rods in the image volume. We show an example image volume at 1.85 V in Figure 7a that is highly ordered and from which the centroid locations were taken. From these data, we calculate the density distribution as a function of height (z -axis). The density plot in Figure 7b shows a periodic rod density at $0.5D$ indicating alternating layered structure. A simple structure that has such a periodicity is a body-centered tetragonal (bct) lattice (e.g., Figure 7c). We further investigate the periodicity of assembly via the static structure factor $S(q)$ for the assembly experiments along the normal (z -axis) to the electrode surface and compare them to the Bragg peaks of the bct lattice. We calculate the $S(q)$ over a range of wavenumbers along the q_z reciprocal lattice from the centroid data. We observe a strong peak at $q_z = 12.3/D$ (Figure 7d), which corresponds to spacing of $0.51D$. This peak indicates the presence of layered positional order in the sample along an axis normal to the electrode surface. The layers are periodically arranged at a distance of about half the minor axis width of the rods or $0.5D$. We note that the diminished higher harmonics in $S(q)$ of the data is due, in part, to separate oriented domains (see SI). If we restrict the scattering to specific domains we see an emergence of a harmonic peak at $q_z \approx 25/D$ (see SI). At both lower and higher Pe , diffuse and jammed structures did not show such positional order.

For comparison, we created representative renderings of the known spheroidal assemblies predicted by self-assembly simulations, shown in Figures 7e, 7f and 7g. Possible structures that might include layered ordering and be consistent with the measured volume fraction of 49% are the smectic C phase with an interlayer distance of the minor axis (D) (Figure 7e), face-centered orthorhombic (fco) as simulated by Frenkel and Mulder^[6] with an interlayer distance of $0.92D$ (Figure 7f), and the monoclinic spheroidal $mC2$ phase of Pfeleiderer and Schilling^[14] with an interlayer distance of $0.6D$ (Figure 7g). A rendering of a body-centered tetragonal (bct) phase that is consistent with experiments showing positional ordering is shown in Figure 7h. In particular, the render shows a layer spacing of $\sim 0.5D$, a high order parameter ($S = 1$), and a volume fraction of 49%. We remark that the spacing of the $mC2$ phase rendered in Figure 7g could be consistent with the experiments (Figure 7b) yet require higher densities to form than were achieved in the experiments.

3. Discussion

The application of a DC electric field across a colloidal suspension of polystyrene spheroidal particles dispersed in DMSO led to a rapid increase in concentration of the particles at the oppositely charged electrode surface (<1 h). At low voltages, the electric field induced the formation of diffuse, disordered structures of the rods. At intermediate voltages the volume fraction was high enough and the kinetics of the assembly sufficiently favorable that large-scale nematic structures with high

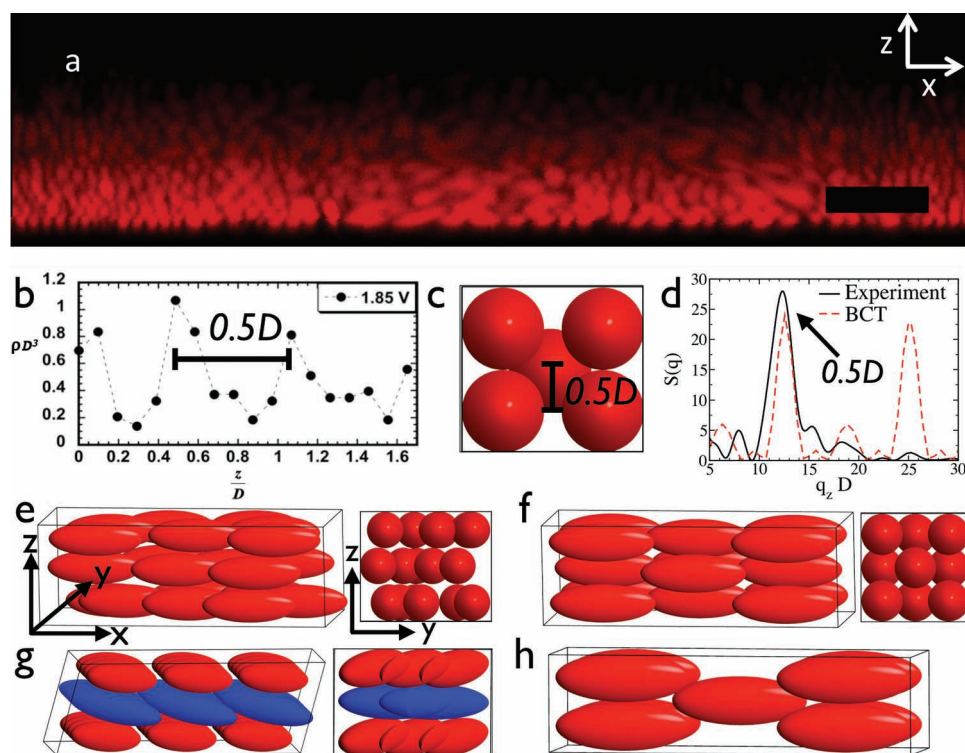


Figure 7. The positional order of the rods for the optimal assembly voltage is shown for layers nearest to the electrode surface. a) A CLSM image taken perpendicular to the coverslip showing the layered structure (scale bar 10 μm). b) Plot of the experimental density profile obtained by means of image processing. It shows a spacing of $0.5D$ between successive rod layers. c) Rendering of a lattice with such spacing (taken from the BCT structure shown in h). d) We compare the rod assemblies to the BCT lattice via the static structure factor $S(q)$. At 1.85 V we find a peak at $q_z = 12.3/D$ corresponding to a layering distance $z = 0.51D$. Additionally, we plot the Bragg peaks of the BCT lattice and we find good agreement for the range of wavenumbers. For comparison, we show renderings in two perspectives of the known phases for hard ellipsoids (e–g) and the BCT phase in (c,h). All renderings in panels (e–h) are shown for volume fractions of 49%.

orientational order formed. Finally, at high voltages, although the volume fraction was high, the kinetics of the assembly did not lead to equilibration into large-scale ordered structures, and disordered glassy structures formed instead. The experiments require a greater field strength to achieve a given order parameter and volume fraction than a simple theory of field-assisted assembly predicts. We experimentally verified that the primary effect of the DC field was to facilitate rapid concentration of an initially low volume fraction sample of spheroids. This concentrating effect was sufficient to induce equilibrium phase transitions. The densest assembly displayed phases with high orientational order ($S = 0.77 \pm 0.06$) and positional ordering consistent with efficient packings of spheroids. The order parameters reported in this paper are comparable or better to previous literature reports. For example, Mukhija and Solomon, using rigid rods of a similar aspect ratio, reported a best order parameter of 0.58 by the method of centrifugation. A very high order parameter ($S = -0.85$) for rod shaped colloidal particles was reported by Dogic et al. for the case of semi-flexible fd virus rods and a depleting polymer at high aspect ratios (~ 130)^[42] This discussion section focuses on the electrochemical mechanism that drives the electrophoresis, as well as the action of the electric field in facilitating the self-assembly. The unexpected lateral positional order observed for some of our samples is also discussed.

DC electric fields can lead to electrohydrodynamic flows^[33] and electro-osmotic flows^[39] in addition to the electrophoretic motion of the colloids themselves. Each effect can influence the structure of the final assembly. For example, Trau et al.^[33] reported that electrohydrodynamic flows lead to lateral motion of the particles along the electrode surface, which leads to formation of 2D aggregates that crystallized over time. By contrast, in our system, direct visualization by CLSM in planes both parallel and perpendicular to the electrode surface showed no significant lateral motion of colloids. Instead, the principal observed motion was perpendicular to the electrode surface, consistent with electrophoresis.

The observed electrophoretic motion is driven by an electric field, the magnitude of which is proportional to the current density across the gap between the electrodes. The current density is not created by double-layer charging, since the millisecond time scale for developing the double layer is much faster than the observed relaxation of i . Instead, the exponential increase in i with applied voltage as seen in Figure 5 is consistent with a Faradaic process at the electrode, i.e. a heterogeneous chemical reaction. Depletion of the reactant undergoing this chemical reaction sets up ionic mass transfer toward the electrode, which leads to the observed i . The observed decay of i over time for an applied voltage is consistent with the reactants diffusing to the electrode

surface. It is our hypothesis that dissolved oxygen and/or water in our solvent are the reactants that ultimately drive the field-assisted assembly process. For example, a $5 \mu\text{A}/\text{cm}^2$ current density would require a dissolved impurity concentration of $\sim 1 \text{ mM}$.^[38] This concentration is reasonable: for example, oxygen dissolved in DMSO is $\sim 0.75 \text{ mM}$.^[43] Further, i decreases as the available concentration of reactants is depleted at the electrode due to the chemical reaction and mass-transfer limited diffusion of reactants from the bulk. Thus, the depletion of residual reactants from the cell due to the electrode reaction explains the time dependence of the measured current reported in Figure 5.

We attempted to affect the electric field driving force for assembly by changing the concentration of water and dissolved oxygen in the assembly device. The experiment was conducted in a glove box where the oxygen had been purged from anhydrous DMSO. In this case, the current density generated upon application of a constant 2.75 V in the solvent was at least a factor of 8 less than reported at the same voltage in Figure 5. The lower i is explained by the lower concentration of oxygen and water reactants, which had been partially removed from the system. This further justifies our hypothesis that oxygen and water are the reactants responsible for the evolution of current in the system.

In Figure 6, we compare the measured equation of state in our field-assisted assembly system using the relation of Equation 1 to that of an equilibrium simulation of hard prolate-spheroids. The Pe required to generate the reported volume fractions and order parameters at the cover slip in the experiments were ~ 10 times larger than the theory predicted. This discrepancy was observed earlier for colloidal rods assembled using the centrifugal force (although it was more pronounced in that case).^[18] In the present work, the theory was able to predict the sharp increase in experimental order parameters near the nematic order–disorder transition volume fraction. Further, there was an excellent correlation between the observed volume fraction and order parameters with volume fractions and order parameters calculated theoretically. Thus, even though the external force needed to assemble ordered structures was larger than expected, the behavior of colloids in the DC electric field device is consistent with a mechanism of self-assembly and equilibrium phase transitions. The larger external force may be required to overcome the increased osmotic pressure due to charge repulsion and excluded volume interactions between ions in the experimental rod system. Further, particle number density effects on rotational and translational dynamics might require higher effective Pe to achieve ordering than predicted by the simple theory that is valid for $\text{Pe} < 1$. Finally, the time-dependent electric-field driving force complicates the comparison to the steady-state theoretical results.

An additional deviation from theory is that at high Pe, we observe the formation of disordered, jammed structures. This result contradicts the prediction that as the field strength is increased; the colloidal volume fraction ought to increase to the point that crystalline structures form.^[35] We attribute this discrepancy to the formation of jammed structures, which prevent formation of the high degree of orientational ordering required to achieve the densest, crystalline assemblies. A first

possible mechanism, which could lead to formation of these jammed structures, is that at high Pe the kinetics of the electrophoretic deposition is too rapid relative to orientational relaxation times to allow the specimens to self-organize into crystalline arrays. Attention to the effect of increased volume fraction (or effective viscosity) on the rotational diffusivity of rods in a uniform velocity field would help address this potential effect. A second possible mechanism is that the Pe are sufficient to densify the suspensions above their glass transition volume fraction. Yatsenko and Schweizer^[44] predicted a glass transition volume fraction of 32% for an aspect ratio of ~ 4 . The high field experiments all result in assembled structures with volume fractions larger than this glass transition volume fraction. In future studies, through measurements of the mean-squared displacement, the approach to the glass transition could be determined quantitatively.

We also observe formation of domains and grain boundaries in the nematic phases. For example, the average domain size is $\sim 680 \pm 120 \mu\text{m}^2$ for the applied voltage of 1.85 V in the plane parallel to the electrode surface. Qualitatively, the domain size is observed to be a strong function of the applied voltage, as apparent in Figure 4. It is interesting to consider the future possibility that larger nematic domains might be produced through variation of the applied voltage, as in annealing. Moreover, future quantification of the nematic texture would more definitively address the question of spatial persistence of local order in the colloidal rod suspensions.

Under optimal assembly conditions (1.85 V) we find that the density of the assembly varied periodically as a function of height leading to positional and orientational symmetries. In Figure 7d we plot the structure factor along the z -axis for the nearest four layers and find periodicity at $q_z = 12.3$ or $z = 0.5D$, which recovers the 0.5D layers seen in the spheroidal number density in Figure 7b. This periodicity suggests that these conditions induce the formation of a body-centered tetragonal (BCT) phase with spheroids layered in alternating fashion (Figure 7c,h). For comparison, we overlay the $S(q)$ for a BCT lattice of spheroids (see Figure 7c). An interlayer spacing of 0.5D suggests that other known ordered phases are not commensurate. For example, in smectic structures this spacing is expected to be no less than the minor axis of the rod (Figure 7e).^[35] Alternatively, the interlayer spacing of the crystal structure of spheroids studied by Frenkel and Mulder was 0.866D at a volume fraction of 74% (Figure 7f).^[6] For a volume fraction of 49% (equal to the experimental volume fraction), this crystal would have an interlayer spacing of 0.94D. Pfeleiderer and Schilling observed even denser spheroidal crystals with an interlayer spacing of 0.5D (Figure 7g) at a volume fraction of $\sim 77\%$.^[14] For a volume fraction of 49% this interlayer spacing would be 0.6D. Finally, it is interesting to note that the BCT phase has not been previously predicted in equilibrium self-assembly of hard spheroids, although there is evidence of the BCT phase in the assembly of anisotropic colloidal particles such as heterodimers.^[45,46] While the observed interlayer spacing of 0.5D and the high order parameter ($S = 0.77$) are consistent with the BCT structure, we cannot say whether the emergence of the BCT phase is a field-induced phase or a non-equilibrium phase. Further

studies are necessary to be able to distinguish the effect of the field on the phase diagram of the ordered rods.

Finally, we note that although we used an electric field to drive the particles to higher densities, the system is suitable for the study of equilibrium self-assembly. Most field-assisted assembly studies reported to date have used time invariant driving forces that are described by the action of a fixed gravitational force on the colloids during assembly.^[18,35] Even with a constant voltage DC electric field, the method discussed in this paper produces a time varying driving force on colloidal particles, as demonstrated by results in Figure 5. The origin of the time-varying force is most likely the temporal evolution of the electric field due to transport phenomena and electrochemical reaction of residual reactants at the electrode surface. This driving force is initially high and thus leads to rapid accumulation of colloids at the surface, a process that is advantageous for accelerated assembly kinetics. Next, as the residual reactant is depleted from the cell, the driving force becomes relatively small and nearly constant due to the lower effective field strengths. At this stage, a further gradual increase in volume fraction occurs. The relative magnitude of the applied field is now comparable to Brownian motion ($Pe \sim 1$). This congruence facilitates rearrangement and the efficient formation of ordered structures. On the contrary, if the driving force remains high after the initial deposition stage, as in the case of an applied initial voltage of between 2 and 3 V, jammed structures form instead of oriented arrays.

4. Conclusion

We have used DC electric fields to induce highly oriented ordered spheroidal phases in an initially low volume fraction colloidal rod suspension. We see a strong correlation up to intermediate voltages (~ 1.85 V) between experimental and theoretically reported order parameter and the volume fractions. This correlation suggests that the assembly is controlled by equilibrium thermodynamics. The method introduced in this paper is broadly applicable to the controlled self-assembly of colloidal particles. As opposed to other field-assisted assembly methods, such as sedimentation or centrifugation, the method provides a natural way to controllably vary the applied field over the course of the experiment. Moreover, it is a versatile method that requires only a small number of particles to study the kinetics and statistical thermodynamics of the assembly process. The method is an excellent candidate for the assembly of colloids such as Janus particles^[47] that are often only available in limited quantities and this method has only small material requirements. Anisotropic particles have complex shapes and potential interactions and hence optimization of kinetic pathways might be required to successfully assemble particular target structures. Due to the scope for programming the applied field strength in this device, the electric-field assembly method described here provides flexibility to select particular kinetic pathways for assembly.

5. Materials and Methods

Monodisperse Spheroid Synthesis: We synthesized spheroidal PS particles by mechanically stretching 1.10 ± 0.02 μm

diameter spherical carboxylate modified polystyrene (PS) particles (Fluospheres F8820, Invitrogen Inc) embedded in a polyvinyl alcohol (PVA, Sigma Aldrich, 30 000–70 000 molecular weight) matrix at a temperature above the glass transition of the spheres. PS microsphere solution in water (2 vol%, 300 μL) was mixed with PVA stock solution (10 wt% PVA, 7.5 mL). This mixture was allowed to dry overnight in flat omni trays. The trays were placed on leveling platforms to ensure thin film formation of uniform thickness. The dried films (thickness = ~ 40 μm) were then peeled from the tray and cut into strips. These strips were placed in a custom stretching device, which was housed in an oven. The oven was heated to 120 $^{\circ}\text{C}$, which is above the glass transition temperature of polystyrene ($T_g \sim 100$ $^{\circ}\text{C}$). This temperature was maintained for ~ 10 min to ensure uniform heating. An elongational strain of 2.5 was then applied to the films so as to obtain a final aspect ratio of 4.3. The stretched portions of the PVA strips were cut out and placed in distilled water for 24 h to dissolve the PVA matrix, thereby releasing the spheroidal particles. The particles were dispersed in DMSO by solvent transfer to yield a solution with an initial volume fraction (ϕ_i) of 2.0 vol%. TBAC (0.1 mM, Fluka) was dissolved in DMSO to control the Debye length of the solution. The rod dimensions were characterized using a Scanning Electron Microscope (Philips XL-30). Zeta potential measurements were done for a dilute rod suspension (~ 0.5 vol%) using a Nano-ZS (Malvern Instruments) to calculate the charge on the colloidal particles.

DC Electric Field Assembly Device: Thin glass cover slips (Fisher Scientific, 12545-G) were coated with a thin layer of indium tin oxide (ITO, ZC&R Inc). The ITO coating was sufficiently thin (~ 10 nm) that high-quality confocal microscopy images could be acquired across the electrode. Two such cover slips were used to make the electric field device. To separate the electrodes, we created spacers from 1 mm thick microscope cover slips. We drilled a 1 cm hole in the center of the spacer to create a chamber for the colloidal suspension. We also glued T2 thermocouple wires (0.5 mm diameter, Goodfellow Inc) to the ITO coated cover slips using silver epoxy (MG Chemicals). This created a conductive connection to the ITO layer. We used UV curable glue (Light weld, Dymax Corporation) to glue the spacer between the two cover slips (ITO coating facing the solution side). A small (1 mm diameter) hole was drilled through the top electrode to allow solution to be injected into the sample chamber. We ensured that no air bubbles were present upon introduction of the colloidal suspension by slowly filling up the chamber and sealing the hole with a small piece of glass coated with vacuum grease. In this paper, the solvent for assembly was DMSO; however, experiments in solvents of different polarities (e.g. ethanol and a mixture of cyclohexylbromide-decalin) showed similar results.

In Situ Characterization of Assembly Structure and Kinetics with Confocal Microscopy: The electric field device was placed on the stage of a confocal laser-scanning microscope (Leica TCS SP2), and the leads were connected to a potentiostat (Autolab PGSTAT 128N). The cover slip directly above the objective was given a positive polarity, while the top cover slip was given a negative polarity. The potentiostat was programmed to apply a constant voltage across the colloidal

suspension, while simultaneously measuring the resulting current density. We studied the kinetics of assembly in planes both parallel and perpendicular to the electrode surface, by taking images at a maximum of 0.657 s per frame using a 100X oil immersion objective (NA 1.4). The experiment was performed for at least 1 h.

For some experiments, we added 1 wt% initiator (Irgacure 2100, Ciba Speciality) and 5 wt% photopolymer (trimethylolpropane triacrylate esters, Sartomer Inc) to enable immobilization of the assembled structures by photopolymerization.^[22] Photopolymerization was performed for samples with low voltages, which formed diffuse assemblies whose structure could not be captured for successful image processing without photopolymerization. We activated the photopolymer using UV light after a steady-state assembly had been obtained. The photopolymer immobilized the structure within less than 1 s and had a negligible effect on the Debye length and the zeta potential (data not shown).

Quantitative Image Processing and Structural Characterization of CLSM Image Volumes: For characterization of the self-assembled structures by image processing, we acquired image volumes of size $19.63 \mu\text{m} \times 19.63 \mu\text{m} \times 2.5 \mu\text{m}$. The voxel size was $38.3 \text{ nm} \times 38.3 \text{ nm} \times 38.4 \text{ nm}$. These stacks were representative of near wall local order in a particular region. Image processing was used to identify the centroids and directors of all rods in the image volume.^[13] Briefly, after a Gaussian filter had been applied, the program automatically identified the central backbone of the rods as the brightest pixels within a local region of order the half-width of the rod. These backbone pixels were identified as individual rods by cluster analysis. The centroid and the orientation angles of each rod were computed from the set of backbone clusters. The variation in centroidal density from the coverslip was reported in Figure 7 as a function volume fraction. All the orientation angles identified were used to compute the S given by Equation 7 and as shown in Figure 6. We tested the method by comparing the number of particles identified in a specified volume to the known macroscopic volume fraction, as determined by sample weight. The relative error in number of particles identified was 1.5%. Moreover, rod backbones identified by the algorithm were overlaid on Gaussian filtered images to check for the fidelity of the centroidal location and the orientation of the identified backbone. Additional details of the performance of the image processing are available in Dzul et al.^[48]

Supporting Information

Supporting Information is available from Wiley Online Library or from the author.

Acknowledgements

A.A.S. and M.J.S. acknowledge funding from National Science Foundation Nanoscale Interdisciplinary Research Teams (NSF-NIRT 0707383) for initial development of the self-assembly method.

A.A.S., K.L.K., S.C.G., and M.J.S. acknowledge support from the Army Research Office Multidisciplinary University Research Initiative (ARO MURI W911NF-10-1-0518) for application of the method to produce and characterize the highly ordered structures reported here. K.H.A. acknowledges support from the National Research Foundation of Korea (NRF) grant (No. 2010-0027746) funded by the Korea government (MEST). The authors thank Joanna Mirecki Millunchick for use of the potentiostat.

- [1] S. C. Glotzer, M. J. Solomon, *Nat. Mater.* **2007**, *6*, 557.
- [2] U. Agarwal, F. A. Escobedo, *Nat. Mater.* **2011**, *10*, 230.
- [3] P. F. Damasceno, M. Engel, S. C. Glotzer, *ACS Nano* **2012**, *6*, 609.
- [4] Y. Kallus, V. Elser, *Phys. Rev. E* **2011**, *83*, 036703.
- [5] M. J. Solomon, *Curr. Opin. Colloid Interface Sci.* **2011**, *16*, 158.
- [6] D. Frenkel, B. M. Mulder, *Mol. Phys.* **2002**, *100*, 201.
- [7] A. P. Hynninen, J. H. J. Thijssen, E. C. M. Vermolen, M. Dijkstra, A. Van Blaaderen, *Nat. Mater.* **2007**, *6*, 202.
- [8] T. Koschny, L. Zhang, C. M. Soukoulis, *Phys. Rev. B* **2005**, *71*, 121103.
- [9] M. J. Solomon, *Nature* **2010**, *464*, 496.
- [10] C. C. Ho, A. Keller, J. A. Odell, R. H. Ottewill, *Colloid Polym. Sci.* **1993**, *271*, 469.
- [11] K. M. Keville, E. I. Franses, J. M. Caruthers, *J. Colloid Interface Sci.* **1991**, *144*, 103.
- [12] Z. K. Zhang, P. Pfeleiderer, A. B. Schofield, C. Clasen, J. Vermant, *J. Am. Chem. Soc.* **2011**, *133*, 392.
- [13] A. Mohraz, M. J. Solomon, *Langmuir* **2005**, *21*, 5298.
- [14] P. Pfeleiderer, T. Schilling, *Phys. Rev. E* **2007**, *75*, 020402.
- [15] A. Donev, I. Cisse, D. Sachs, E. A. Variano, F. H. Stillinger, R. Connelly, S. Torquato, P. M. Chaikin, *Science* **2004**, *303*, 990.
- [16] A. Donev, F. H. Stillinger, P. M. Chaikin, S. Torquato, *Phys. Rev. Lett.* **2004**, *92*, 255506.
- [17] M. Radu, P. Pfeleiderer, T. Schilling, *J. Chem. Phys.* **2009**, *131*, 164513.
- [18] D. Mukhija, M. J. Solomon, *Soft Matter* **2011**, *7*, 540.
- [19] Z. Dogic, S. Fraden, *Curr. Opin. Colloid Interface Sci.* **2006**, *11*, 47.
- [20] M. P. B. vanBruggen, F. M. vanderKooij, H. N. W. Lekkerkerker, *J. Phys. Condensed Matter* **1996**, *8*, 9451.
- [21] R. Ni, S. Belli, R. van, Rene, M. Dijkstra, *Phys. Rev. Lett.* **2010**, *105*, 088302.
- [22] L. T. Shereda, R. G. Larson, M. J. Solomon, *Phys. Rev. Lett.* **2010**, *105*, 038301.
- [23] J. P. Hoogenboom, P. Vergeer, A. van Blaaderen, *J. Chem. Phys.* **2003**, *119*, 3371.
- [24] A. L. Rogach, N. A. Kotov, D. S. Koktysh, J. W. Ostrander, G. A. Ragoisha, *Chem. Mater.* **2000**, *12*, 2721.
- [25] M. Grzelczak, J. Vermant, E. M. Furst, L. M. Liz-Marzan, *ACS Nano* **2010**, *4*, 3591.
- [26] J. J. Juárez, M. A. Bevan, *J. Chem. Phys.* **2009**, *131*, 134704.
- [27] N. Li, H. D. Newman, M. Valera, I. Saika-Voivod, A. Yethiraj, *Soft Matter* **2009**, *6*, 876.
- [28] S. O. Lumsdon, E. W. Kaler, O. D. Velev, *Langmuir* **2004**, *20*, 2108.
- [29] O. D. Velev, K. H. Bhatt, *Soft Matter* **2006**, *2*, 738.
- [30] M. E. Leunissen, M. T. Sullivan, P. M. Chaikin, A. van Blaaderen, *J. Chem. Phys.* **2008**, *128*, 164508.
- [31] M. T. Sullivan, K. Zhao, A. D. Hollingsworth, R. H. Austin, W. B. Russel, P. M. Chaikin, *Phys. Rev. Lett.* **2006**, *96*, 15703.
- [32] J. P. Singh, P. P. Lele, F. Nettesheim, N. J. Wagner, E. M. Furst, *Phys. Rev. E* **2009**, *79*, 050401.
- [33] M. Trau, D. A. Saville, I. A. Aksay, *Science* **1996**, *272*, 706.
- [34] K. S. Napolskii, N. A. Sapozhnikova, D. F. Gorozhankin, A. A. Eliseev, D. Y. Chernyshov, D. V. Byelov, N. A. Grigoryeva, A. A. Mistonov,

- W. G. Bouwman, K. O. Kvashnina, A. V. Lukashin, A. A. Snigirev, A. V. Vassilieva, S. V. Grigoriev, A. V. Petukhov, *Langmuir* **2010**, *26*, 2346.
- [35] S. V. Savenko, M. Dijkstra, *Phys. Rev. E* **2004**, *70*, 051401.
- [36] W. B. Russel, D. A. Saville, W. R. Schowalter, *Colloidal Dispersions*, Cambridge University Press, Cambridge, Great Britain, **1989**, p. 411.
- [37] M. Teubner, *J. Chem. Phys.* **1982**, *76*, 5564.
- [38] A. J. Bard, L. R. Faulkner, *Electrochemical Methods: Fundamentals and Applications*, Wiley, Hoboken, NJ, **2001**, p. 12.
- [39] Y. Solomentsev, M. Bohmer, J. L. Anderson, *Langmuir* **1997**, *13*, 6058.
- [40] H. Brenner, *Int. J. Multiphase Flow* **1974**, *1*, 195.
- [41] B. Tjijto-Margo, G. T. Evans, *J. Chem. Phys.* **1990**, *93*, 4254.
- [42] Z. Dogic, K. R. Purdy, E. Grelet, M. Adams, S. Fraden, *Phys. Rev. E* **2004**, *69*, 051702.
- [43] R. Henríquez, M. Froment, G. Riveros, E. A. Dalchiale, H. Gómez, P. Grez, D. Lincot, *J. Phys. Chem. C* **2007**, *111*, 6017.
- [44] G. Yatsenko, K. S. Schweizer, *Langmuir* **2008**, *24*, 7474.
- [45] I. D. Hosein, S. H. Lee, C. M. Liddell, *Adv. Funct. Mater.* **2010**, *20*, 3085.
- [46] E. B. Mock, C. F. Zukoski, *Langmuir* **2007**, *23*, 8760.
- [47] Q. Chen, J. K. Whitmer, S. Jiang, S. C. Bae, E. Luijten, S. Granick, *Science* **2011**, *331*, 199.
- [48] S. P. Dzul, M. M. Thornton, D. N. Hohne, E. J. Stewart, A. A. Shah, D. M. Bortz, M. J. Solomon, J. G. Younger, *Appl. Environ. Microbiol.* **2011**, *77*, 1777.

Received: October 27, 2011
Revised: December 12, 2011
Published online: March 1, 2012